Shear Orientation of Nanoparticle Arrays Templated in a Thermoreversible Block Copolymer Micellar Crystal

Danilo C. Pozzo[†] and Lynn M. Walker*

Department of Chemical Engineering (Center for Complex Fluids Engineering), Carnegie Mellon University, Pittsburgh, Pennsylvania 15213

Received January 3, 2007; Revised Manuscript Received April 27, 2007

ABSTRACT: The shear alignment of binary crystals of polymeric micelles and small particles is demonstrated using contrast-variation SANS experiments. The larger micelles form close-packed crystals that serve as a template to the smaller nanosized particles. The simultaneous alignment of the two phases, micelles and templated particles (silica or albumin proteins), is demonstrated from the scattering at two different contrast values. A new method to quantify the alignment of colloidal crystals using diffraction is also proposed. This method is used to probe the alignment of the crystals as a function of shear rate. It is found that the binary crystals align at significantly lower shear rates when compared to the neat micelle crystals. The diffraction profiles of the cocrystals are compared to models for the flow mechanism of colloidal crystals. Differences between the experimental profiles and the predictions suggest that there is a coexisting crystal phase that is not accounted for in the model.

1. Introduction

Like surfactants, amphiphilic block copolymers can form spherical micellar aggregates when they are dispersed in a solvent that is selective to specific blocks in the polymer. When the polymer concentration is sufficiently large, these micelles spontaneously pack into a crystalline lattice due to their repulsive (steric) interaction.[1−4] This crystallization effect is similar to that occurring in concentrated dispersions of solid colloidal particles.[5,6] Under an applied shear field, the micelles or particles that make up a colloidal crystal are able to move and slide past each other as their spatial arrangements are controlled by steric repulsion and not by covalent or other strong bonds. Simple shear has been shown to anneal lattice defects and to align the colloidal crystals so that the bulk of the particles are part of the same lattice and have the same macroscopic orientation.[7−9] Under appropriate shear conditions, it is even possible to obtain a single crystal of spherical micelles.[7]

The purpose of this work is to evaluate the shear orientation of *binary* colloidal crystal nanocomposites. These materials consist of nanometer-sized particle additives, silica or proteins, that are dispersed within an ordered micellar crystal template. The particles, which are smaller than the micelles, partition themselves in the interstitial cavities between the micelles. Therefore, the polymeric matrix acts as a template by imposing its crystalline order on the dispersed nanoparticles that would not self-assemble on their own.[4,10] It is possible to tune the organization of the dispersed additives by altering the structure of the micelle template. The structure of the micelle template may be controlled by a judicious choice of the polymer architecture and solution conditions; a wide range of structures and systems have been reported previously.[1,2,9] By dispersing particles in these micelle templates, the resulting material is a cocrystal of micelles and dispersed particles that is analogous to a metallic alloy. Figure 1 shows a schematic representation of a one-component micellar crystal and the cocrystal that is created by dispersing smaller nanoparticles within the micelle matrix.

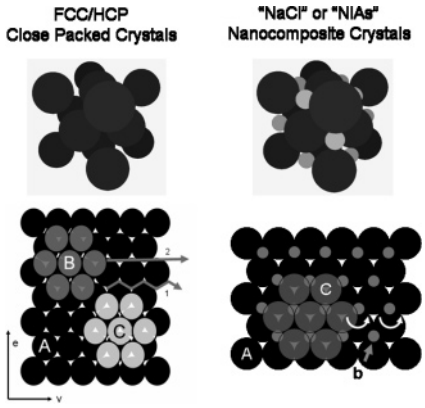

Figure 1. Schematic representation of a close-packed crystal of spherical micelles (left) and of a nanocomposite crystal that is formed when smaller particles are inserted into the octahedral interstitial cavities (right). The lower figures illustrate the stacking of hexagonal planes of particles in the shear gradient direction for both types of crystals. The arrows show the possible sliding mechanisms that occur during shear flow: zigzag (1) and layer sliding (2).

We have recently presented a simple procedure to create these novel composites using thermoreversible polyether block copolymers (Pluronic) as the matrix.[11−13] The thermoreversible micellization of these polymers allows us to disperse particles in concentrated polymer solutions at low temperatures without encountering the dispersion problems that are commonly caused by the high viscosity of the crystalline matrix. Once the particles are fully dispersed, the temperature is raised to induce the formation of the micellar crystal. During this process, the particles are trapped in the solvent-filled interstitial spaces that remain between the micelles and thus form a crystalline array of their own.[12,13] The organization of nanosized particles is a particularly active area of research due to the potential that these materials have in the development of advanced technologies like sensors and nanoelectronics.[14,15] In this paper, we extend our previous work on block copolymer templating by evaluating the alignment of binary crystals using shear. Although we focus on soft polymeric micellar crystals, we expect that the general findings can be extended to other types of cocrystals.[6,16]

* Corresponding author. E-mail: lwalker@andrew.cmu.edu.
[†] Current address: NIST Center for Neutron Research, Gaithersburg, MD 20899.

10.1021/ma0700173 CCC: $37.00
Published on Web 07/07/2007

The shear alignment of single-component micellar and colloidal crystals has been the subject of numerous studies.[5,7−9,17−22] Small-angle neutron and X-ray scattering (SANS and SAXS) techniques have proven to be invaluable tools in assessing the structural order of colloidal crystals due to their ability to probe bulk structures at nanometer length scales during and after shear alignment. We have recently demonstrated, through contrast variation SANS experiments, that this macroscopic shear alignment is also possible in binary crystals of particles and micelles.[13] In this contribution, we provide a thorough description of the shear alignment of these composite materials. We also extend our templating method to the organization of globular proteins.

Small-angle scattering experiments provide information on the static and dynamic structure of aligned colloidal crystals. Unfortunately, extracting structural information from the scattering profiles is often challenging because several factors lead to changes in the scattering intensity. A model to describe the diffraction pattern of close-packed colloidal crystals under shear was developed by Ackerson and Loose.[23] The application of this model has proven to be successful in representing most of the features that arise in the two-dimensional diffraction profiles of close-packed crystals (FCC/HCP) and body-centered-cubic crystals (BCC) under flow.[21,22] Although this model is useful to determine the structure of the shear-aligned crystals, it does not allow for a simple quantification of the level of orientation. Therefore, some important information that is embedded in the scattering is usually lost.

Here we report on the shear orientation of neat micellar crystals and the corresponding binary crystals using SANS under shear. We use neutron scattering to probe these systems because it can be used to independently assess the structure of the micellar crystal and the templated particles through the use of contrast variation schemes.[13] While SANS suffers from low wavelength resolution that generally deters crystallographic studies, the information gained though the advantage of contrast-matching is vital to understanding these binary systems. Furthermore, we present a new and simple method to quantify the level of crystal orientation that does not require fitting of the two-dimensional data and can be applied to other soft crystal systems. We show that this analysis can be effectively used to obtain valuable structural and mechanistic understanding that was previously overlooked.

2. Experimental Section

2.1. Materials and Methods. Samples are prepared as described elsewhere.[11,13] Ludox silica particles of 7 nm nominal diameter (Ludox SM-30) dispersed in water are obtained from Grace Davidson (Columbia, MD) as 30 wt % aqueous dispersions and used as received. Bovine serum albumin (BSA) 98% is obtained from Sigma Aldrich (St. Louis, MO) as a lyophilized powder and is dissolved in water before mixing with the polymer stock solutions. Pluronic F127, F87, and P123 are obtained from BASF (Mount Olive, NJ) and were used as received. The nominal chemical structures for these Pluronic grades are $PEO_{117}PPO_{72}PEO_{117}$, PEO_{78}-$PPO_{48}PEO_{78}$, and $PEO_{21}PPO_{72}PEO_{21}$ respectively. All polymer and particle (silica or protein) dilutions are performed using deionized water (18 MΩ) or 99.8% deuterium oxide D_2O that is obtained from Cambridge Isotopes (Andover, MA). The samples are prepared by mixing the particles in a corresponding amount of water. To this mixture, the required amount of concentrated polymer stock solution is added while it is cold (temperature of an ice bath) and has a relatively low viscosity. The samples are then mixed vigorously and are allowed to equilibrate in the refrigerator or in an ice bath.

2.2. Small-Angle Neutron Scattering. Neutron scattering experiments are carried out at the NIST Center for Neutron Research (NCNR) in Gaithersburg, MD. Data are collected using the 30 m SANS instrument NG3. A mean neutron wavelength (λ) of 6 Å with a spread $\Delta\lambda/\lambda$ of 0.15 is used at sample-to-detector distances of 2 and 4 m. A specially designed Couette shear cell with a 0.5 mm gap is used to collect the data in most of the experiments.[24] Oscillatory shear experiments are carried out using a UDS-200 rheometer (Anton Paar, Graz Austria) that has been configured for SANS measurements. This instrument also uses a Couette geometry with a 0.5 mm gap.[25] The scattering profiles are appropriately reduced to an absolute scale by referencing to the open beam neutron flux after applying the necessary corrections for absorption, empty cell scattering, detector sensitivity, and background signal.[26,27] The absolute scattering cross-section $I(q)$ is collected as a function of the scattering vector $q = |\mathbf{q}| = (4\pi/\lambda)\sin(\theta/2)$, which is a function of the scattering angle (θ) and the azimuthal angle relative to the shear direction.

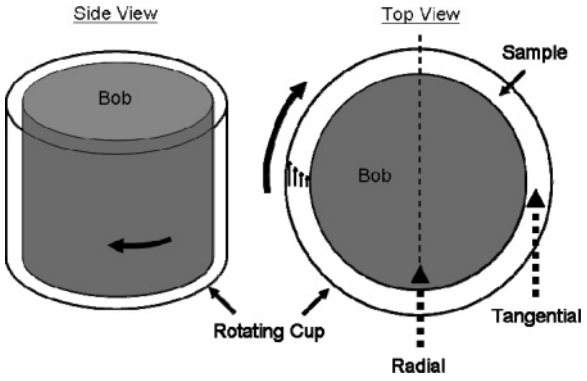

Figure 2. Schematic representation of the NIST shear cell illustration the two scattering geometries that are used in the experiments.

Figure 2 shows the two scattering geometries that are used to probe the structure of the nanocomposites during shear. In the radial geometry the position of the neutron beam is perpendicular to the wall of the shear cell and crosses through the axis of rotation. This geometry probes the structure in the plane defined by the velocity and the vorticity directions. In the tangential geometry, the shear cell is displaced horizontally, and a thin slit is used so that the neutron path is along the gap of the cell. These scattering geometries probe two orthogonal projections of the structure of the samples.

3. Analysis of SANS Profiles

3.1. Structure of Aligned Close-Packed Crystals. In this work we focus on the alignment of close-packed colloidal crystals which form either a face-centered-cubic (FCC) lattice, a hexagonal close-packed (HCP) lattice, or a combination of these two lattices. Micellar crystals will also form other types of lattices, such as body-centered cubic (BCC), and templating of particles in these lattices is also possible. However, the shear orientation and flow of these crystals is more complex than that of close-packed crystals and is beyond the scope of this paper.

FCC and HCP crystals can be created by stacking planes of hexagonally close-packed spheres on top of each other. The specific way that these planes are stacked will determine whether the packing is purely FCC, purely HCP, or a mixture of both lattices. In the case of a mixture, the two primary lattices could be arranged in a number of ways with varying degree of HCP and FCC content. The relative positions of these two lattices could also vary from a homogeneous random mixture to the nonrandom stacking of domains corresponding to each lattice.[28] In this continuum of possibilities, one case corresponds to a homogeneous mixture of hexagonal planes with equal and random occurrence of HCP and FCC stacking and is denoted random close packing (RCP).

When micellar crystals are created in the absence of shear, the initial structure is that of a powder sample where the

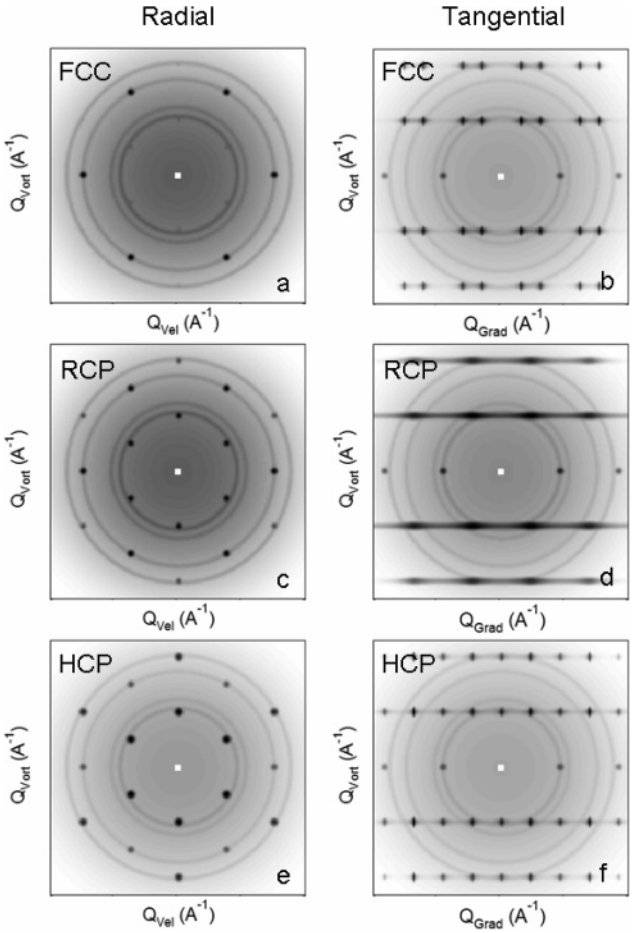

Figure 3. Simulated scattering patterns for face-centered cubic (FCC), random close packing (RCP), and hexagonal close packing (HCP) in the radial (a, c, e) and tangential (b, d, f) scattering geometries. The simulated patterns are for crystals in mechanical equilibrium (at rest).

crystallites have random orientations. It is sometimes difficult to distinguish between FCC and HCP crystals when they have random orientations (powder) due to the low wavelength resolution of SANS experiments. However, during deformation with simple shear, many of the crystallites join together and form a unified lattice. This lattice is usually oriented with the hexagonal planes parallel to the wall of the shear cell. The orientation of the lattice is illustrated in Figure 1. Any given hexagonal plane can take one of three possible equilibrium sites (A, B, and C) as long as it is different from that of the layer above it and the layer below it. An FCC crystal is formed when the stacking of planes follows an ABCABCABC or ACBACBACB sequence. An HCP crystal is created when the sequence is ABABAB, ACACAC, or BCBCBC. An RCP crystal is one that has a random stacking sequence such as ACBCACBABCABC.

In contrast to the powder samples, the scattering from oriented FCC, HCP, or random crystals is quite different, and it is possible to distinguish between them using SANS experiments.[23] Figure 3 shows the predicted scattering profiles for these three lattices in the two common scattering geometries (radial and tangential). The "simulated" profiles are calculated by applying the diffraction model of Ackerson and Loose[23] in a similar way to that described by McConnell and Gast.[21] The lattice structure of the oriented crystals is best probed in the tangential direction. In this geometry, the profiles from the three different lattices show significant differences. However, the lower resolution of tangential scattering profiles makes it difficult to unambiguously extract this information.

The stacking of binary close-packed crystals of micelles and particles with the NaCl or NiAs structure (AB) is also shown in Figure 1. These crystal structures are formed when the small particles occupy the octahedral cavities of the larger micelle crystal. It must be pointed that small particles could also occupy other sites (e.g., tetrahedral sites) resulting in different structures. Some of these (e.g., zinc blende) can also lead to similar diffraction profiles in the crystal orientations that are probed in this work. This makes it impossible for us to exclude other possible lattices solely on the basis of our experiments. Nevertheless, theoretical calculations show that NaCl and NiAs are the most energetically favored structures for the relative particle sizes used in this work.[29] Therefore, we analyze our data on the basis of the assumption that the smaller particles occupy the octahedral sites (NaCl and/or NiAs structures). Crystallographic examination at various crystal orientations, which can be measured by rotating a plate−plate shear cell, could possibly yield the exact lattice of the binary crystal.[9]

An oriented binary crystal can also be formed by stacking hexagonal planes of particles. For these binary crystals, the hexagonal layers of micelles will be in close packing while the layers of small particles will have the same separation distance as the large particles (micelles). The layers of micelles in these binary crystals are packed following the same rules of the neat micelles that form FCC, HCP, or RCP crystals. The equilibrium site for a layer of small particles is then determined by the stacking of the micellar layers that lie above and below. Therefore, a possible stacking sequence of an RCP binary crystal is given by A**b**C**a**B**a**C**b**A**b**C**a**B**c**A**c**B**a**C**b**A**c**B**a**C. The layers of small particles are represented by lower case letters.

Hunt and co-workers calculate the scattering that is expected from binary close-packed crystal lattices (NaCl or NiAs structures) at intermediate contrast conditions (without contrast matching).[30] They find that the relative position of the Bragg peaks in the binary lattices is identical to that of the single-particle FCC/HCP crystals. The interference between the larger and the small particles will only cause small changes in the relative intensity of the peaks. Therefore, no "extra" peaks are expected in SANS experiments that are carried out at conditions where all the components are scattering (isotope mixtures that are away from contrast matching conditions). Consequently, the best way to corroborate the formation of a close-packed binary crystal lattice is to completely suppress the scattering from one of the phases using contrast matching techniques. At these conditions, a single component crystal will not show scattering or Bragg diffraction.[31] In contrast, the diffraction pattern should persist in the case of an ordered binary lattice. For this reason, we perform our experiments at solvent isotope compositions that completely match the scattering contrast of the polymer (12% D_2O and 88% H_2O) or the particles (61% D_2O and 39% H_2O for silica or 40% D_2O and 60% H_2O for the BSA proteins). The contrast matching points are experimentally measured and verified with samples under shear. There is no residual scattering intensity at these conditions. Again, this contrast matching allows us to extract structural information from each individual phase (micelle template or dispersed particles).

3.2. Flow of Aligned Close-Packed Crystals. The flow mechanism that is commonly accepted for single-component micellar crystals is that of sliding layers. At low shear rates, the hexagonal planes that make up the crystal slide past each other by hopping between the equilibrium sites in a zigzag conformation. At higher shear rates, the layers begin to slide in a linear fashion along an intermediate position between these sites. These two trajectories are schematically depicted in Figure

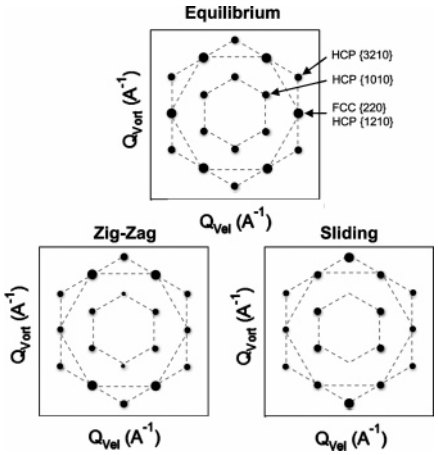

Figure 4. Schematic of the diffraction structure factors that are predicted to occur in the radial scattering geometry by the model of stacked hexagonal layers for an equilibrium structure (rest) and for zigzag and sliding layer flow mechanisms (Figure 1).

1 as paths 1 (zigzag) and 2 (sliding layers). These two mechanisms create anisotropic intensity features in the diffraction patterns that are described in detail by Ackerson and Loose and are qualitatively summarized in Figure 4. In this work, we use the term "anisotropy" to refer to differences in the intensity of Bragg spots that lie at the same magnitude of the scattering vector $|\mathbf{q}|$.

The scattering model for colloidal crystals under shear predicts a decrease in the intensity of the top and bottom Bragg peaks in relation to the four remaining "side" peaks of the first-order hexagon. The model predicts that this peak anisotropy will be observed during the zigzag flow mechanism. During the layer sliding flow mechanism, the model predicts a complete suppression of the top and bottom Bragg peak. A similar change is also predicted to occur in the second-order hexagon, but in this case it is the two side peaks that have a lower intensity. By comparing the peak intensity of the spots in the first hexagon, it is possible to obtain information on the flow mechanism of the crystal.[23] Nevertheless, it is important to keep in mind that the diffraction model assumes that all of the layers in the material have the same flow mechanism. In a real system, it is likely that different fractions of the layers experience different flow mechanisms at the same time. This would result in a linear combination of the scattering profiles shown in Figure 4 and can prevent the unambiguous determination of the details of the flow mechanism. Furthermore, it is important to note that the model predictions are based on an assumption of the amount of time that the hexagonal layers spend at every position during the displacement path of a particular flow mechanism.[23] This is necessary because the intensity that is measured during a shear run is a weighted average of the scattering from all of these intermediate structures. These averaging effects are eliminated when SANS experiments are performed at rest directly after shear alignment. Still, it is essential that this is taken into account when experimental data under shear is compared to existing flow models.

To quantify changes in the scattering patterns, we define a simple anisotropy factor that is calculated from the intensities of the Bragg spots in the first hexagonal ring and normalized by the intensity of the unoriented sample (I_{powder})

$$A = \frac{\bar{I}_{top-bot} - \bar{I}_{sides}}{I_{powder}} \quad (1)$$

According to the flow model,[23] the average intensity of the top and bottom peaks will only be equal to or lower than the intensity of the side peaks. Therefore, according to the flow model of HCP/FCC crystals, A is expected to take a value of zero or to be a negative number.[23] The powder intensity (I_{powder}), which is used to normalize this difference, is collected from the circularly averaged scattering profile of the samples before shear alignment. Alignment caused by loading the sample is erased by melting the crystal at low temperature and re-forming it with a step increase in temperature.

We also propose a new way to quantify the degree of shear alignment of colloidal crystals. In this method we assume that the samples are composed of a fraction of their volume which is perfectly aligned with the shear field while the remaining fraction of the sample is randomly oriented and thus consists of a powder. The scattering from these samples is given by

$$I(q) = B(\Delta\rho,C)\, P(q)[(1 - \phi_P)S_A(q) + \phi_P S_P(q)] + \text{bkg} \quad (2)$$

In eq 2, the factor B lumps the contrast and the concentration terms, $P(q)$ is the form factor of the spherical micelles, ϕ_P is the volume fraction of the sample that is in the powder or disoriented form, $S_A(q)$ is the structure factor of the aligned crystal, $S_P(q)$ is the structure factor of the powder, and bkg is the incoherent scattering background measured at high q. Since $S_A(q)$ is only large near a Bragg spot, it can be assumed to be close to zero when one is sufficiently far from one of these points. Therefore, by analyzing the intensity at a value of the scattering vector (q') that lies in the powder ring but is far from the Bragg spots, it is possible to estimate the volume fraction of sample that is not aligned with the shear field

$$\frac{I_{aligned}(q') - \text{bkg}}{I_{powder}(q') - \text{bkg}} = \frac{(1 - \phi_P)S_A(q') + \phi_P S_P(q')}{S_P(q')} \approx \phi_P \quad (3)$$

This simple analysis is robust and does not require prior knowledge of the form factor of the micelles or any of the contrast and concentration terms as they cancel in the calculation. In practice, we perform an annular average of the intensity at the q value that corresponds to the first-order ring (or hexagon) and compare the intensity of the deepest valleys with the intensity of the sample in the powder state. The magnitude of the ϕ_P, calculated from this analysis, is an overestimate because there is some residual intensity from nearby Bragg spots. Furthermore, quantitative measurement of ϕ_P is affected by other factors including changes in the crystal size, instrumental smearing, and dynamic fluctuations of the micelles. All of these factors will affect the width of Bragg peaks and the quantitative determination of ϕ_P. Nonetheless, the changes in the anisotropy factor A (eq 1) and in the powder fraction ϕ_P (eq 3) as a function of shear rate, sample composition, and other parameters provide valuable information that has not been quantified in other soft crystal systems.

The flow mechanism of the binary crystals that are studied in this work is more complex than that of the single-component crystals. The small particles of the composite crystals occupy the sites that would be visited by the micelles during the zigzag flow mechanism. Therefore, it is expected that the particle additives will create a significant disturbance in the flow mechanism of the micelles. This is possibly the cause of the increase in the modulus that has been observed, and previously reported, when small amounts of additives are added to the micelle crystals.[11] In Figure 1, we postulate an alternative flow mechanism for these binary crystals. In this mechanism, the

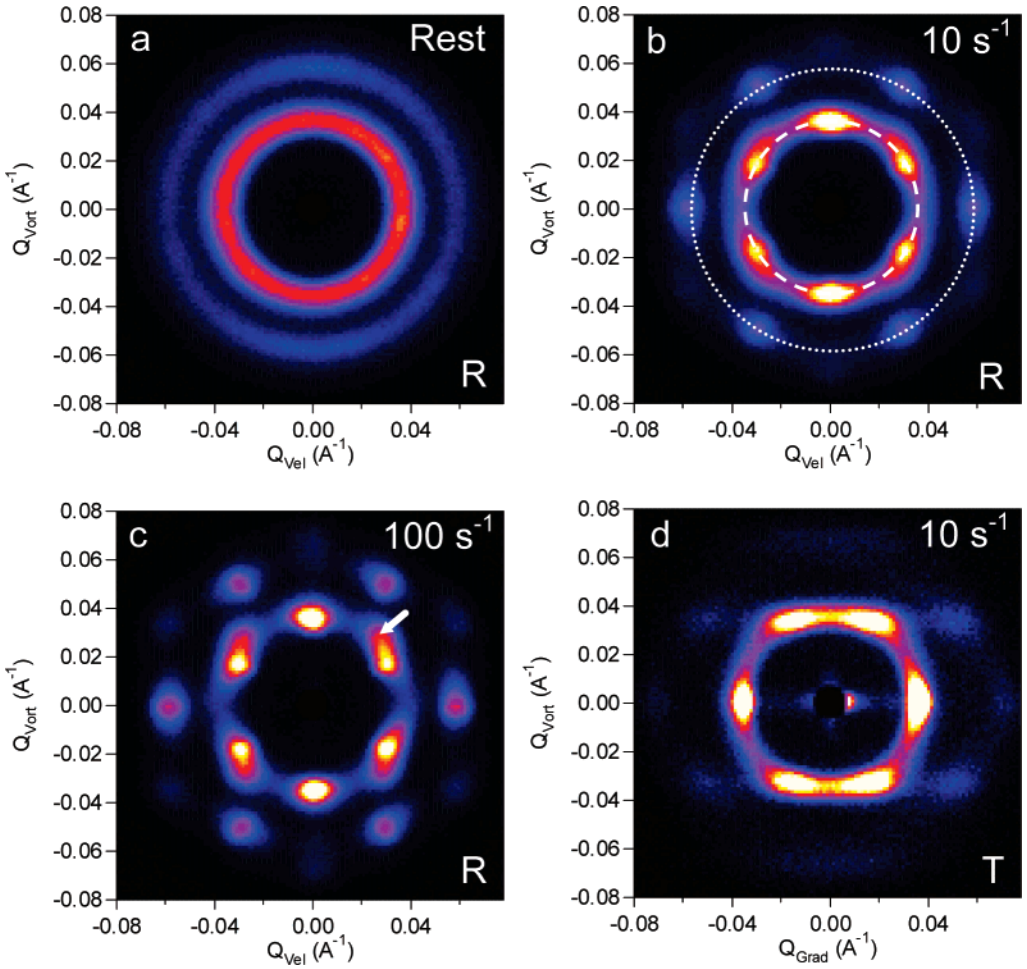

Figure 5. Typical two-dimensional scattering profiles obtained for a sample containing 25 wt % F127 in 100% D2O at 25 °C. The scattering is shown in the radial geometry at rest (a) and shearing at a rate of 10 s^{-1} (b) and 100 s^{-1} (c). The scattering collected in the tangential geometry is also shown for the shearing sample at 10 s^{-1} (d). The dashed lines in (b) show the path for the azimuthal averages of the first and second rings.

micelle layers would "jump" between identical sites through an intermediate position. This alternative displacement could be favored when the small particles are large enough to significantly disturb the zigzag or layer sliding flow mechanisms. When the particles are very small, the traditional flow mechanisms are most likely still favored. We also note that other alternative flow mechanisms could be possible. Still, the flow of binary crystal lattices (NaCl or NiAs) is less understood than that of single-component crystal lattices (FCC, BCC, or HCP), and the diffraction patterns for these alternatives are not currently known.

To obtain information on the shear alignment of binary crystals, we analyze the data of the two phases of the binary crystals using contrast matching experiments. To further quantify the results, we calculate the anisotropy factor (A) and the powder fraction (ϕ_P) for scattering profiles corresponding to the polymer micelle phase.

4. Results and Discussion

4.1. Single-Component Crystals. The experimental scattering profiles for a sample containing 25 wt % Pluronic F127 with no dispersed particles are shown in Figure 5. Figure 5a−c corresponds to the scattering in the radial geometry at various shear rates while Figure 5d corresponds to the tangential scattering. At rest (Figure 5a) the sample is formed without any preferential orientation, and the scattering is mostly isotropic. When the sample is sheared at 10 s^{-1} (Figure 5b) and at 100 s^{-1} (Figure 5c) the expected hexagonal patterns of spots are observed. Three hexagonal rings corresponding to the families of planes of the FCC/HPC crystals are clearly distinguished, and their position is the same that is predicted by the model (Figure 3). Figure 5d shows the scattering pattern that is collected in the tangential geometry at a shear rate of 10 s^{-1}. The patterns in the tangential geometry have a lower resolution than those in the radial geometry due to the use of a thin slit and to the curvature of the cell. Still, the pattern has a structure similar to that of Figure 3d for a random hexagonal close packing (RCP).

At first glance, the scattering profiles in the radial direction appear strikingly similar to the predictions of the Ackerson and Loose model,[23] but a closer inspection reveals that there are important differences. In the experimental scattering profiles (Figure 5b,c), the most obvious deviation from the model is that there is a larger intensity of the top and bottom spots with respect to the four spots of the first-order hexagon. This type of peak anisotropy is not predicted by any of the expected flow mechanisms or structures (FCC, RCP, HCP).[23] This inconsistent profile has been observed experimentally in the past, but it has been given little attention (Figures 4d and 7c,d in McConnell et al.[21]). McConnell and co-workers suggest that this effect could be due to an anisotropic paracrystalline distortion of the lattice during shear or also to the breakup of hexagonal layers in the direction of shear. Although these two effects could potentially lead to this type of anisotropy, they are unlikely causes because the anisotropy in the intensity persists after flow stops. We suggest that the unexpected anisotropy is instead due to a stable

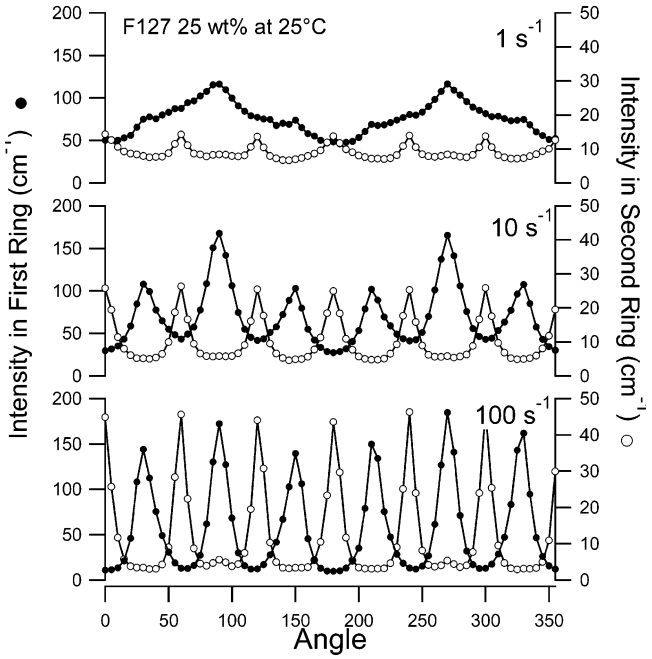

Figure 6. Azimuthal angle average of the intensity of the sample in Figure 5 along the first (closed circles) and second (open circles) hexagonal rings. The angle is measured with respect to the velocity vector. The top Bragg spot of the first-order ring occurs at 90° and the bottom spot at 270°.

coexistence of more than one crystal orientation. This would lead to a different intensity pattern from the predictions of the model, which assumes a single orientation for the entire sample.[23] The coexistence of micelle cubic crystal phases with different lattices and orientations in the same sample has been observed in the past.[8,32,33] The asymmetry in the scattering is more clearly observed in the intensity variation along the azimuthal angle within the first hexagon, as shown in Figure 6. In this figure, the azimuthal angle is defined with respect to the shear, or velocity, direction. The asymmetry of the spots becomes smaller at higher shear rates. This indicates that the crystal may be closer to the structures predicted by the Ackerson and Loose model (Figures 3 and 4).

There is another subtle detail in the radial scattering profiles that further suggests more than one coexisting crystal orientation during flow and after flow. This is the appearance of four "extra" spots in the radial geometry at high shear rates (<100 s^{-1}) and at rest after these high shear conditions. One of these spots is marked with an arrow in Figure 5c. The q position of these spots is consistent with the diffraction of the {200} planes of an FCC crystal. Park and co-workers observe "extra" spots for a similar FCC/HCP crystal in an experiment where the scattering plane is defined by the velocity and the shear gradient directions. They suggest that the "extra" spots are due to a pure FCC phase that coexists with a "mixed" FCC/HCP phase but has a different orientation.[8] A coexisting pure FCC phase with an FCC/HCP crystal is also observed by another group.[32] While we are unable to unambiguously determine the lattice and orientation of these coexisting crystals, the SANS results indicate that the structure and flow mechanism of these systems is significantly more complex than the sliding-layers flow mechanism.[23]

4.2. Binary Close-Packed Crystals. The 2D scattering profiles for a silica nanocomposite under shear are shown in Figure 7. The top three figures (a−c) show the scattering from the silica particles within the composite while the bottom figures (d−f) show the scattering from the micellar template in the same composite. As expected, before shearing the sample, the scattering corresponds to powder scattering with no sign of hexagonal patterns (Figure 7a,d). In contrast, when the sample is sheared at a constant rate of 10 s^{-1}, there is a high degree of alignment on the micelle crystal phase (Figure 7e). The scattering corresponding to the silica particles at the same shear condition (Figure 7b) also shows the formation of a hexagonal pattern. The high intensity in the scattering corresponding to the silica at low q values (Figure 7a−c) is due to the form factor of the particles that are somewhat polydisperse. Despite this high intensity at low q, the hexagonal pattern is still clearly visible. This feature is a clear indication of the alignment of the dispersed silica particles in the nanocomposite. The formation of a hexagonal pattern with the same orientation and peak position as that of the micelle crystal is consistent with the particles being located in the large interstitial sites (octahedral) of the micelle crystal. Still, it is expected that the quality of the crystal formed by the dispersed particles will be significantly lower than that of the micelles because of possible vacancies and defects. The appearance of this hexagonal pattern also indicates that the overall lattice of the templated silica particles is not purely FCC but rather a mixture of FCC/HCP or pure HCP. A pure FCC crystal of the templated particles would not show a diffraction pattern in the innermost hexagon (as shown in Figure 3a).[23]

A somewhat unexpected feature of the diffraction pattern from the micelle crystal phase is the anisotropy in the intensities of the Bragg spots. The azimuthal average of the intensity of the first and second hexagonal rings is shown in Figure 8 for various shear rates. Unlike the diffraction patterns for the pure micelle crystal (Figure 5), this pattern shows a lower intensity for the top and bottom spots with respect to the other four side spots. This type of anisotropy is similar to that which is predicted by the layer sliding model for the zigzag and layer sliding flow mechanisms.[23] Therefore, it appears that the silica nanocomposite follows the predictions of the model while the micelle crystal shows the opposite effect (Figures 5). These results could suggest that the addition of silica particles triggers zigzag or sliding layer motion at lower rates while the neat polymer crystal may show a different flow mechanism at the same shear conditions. The data from McConnell and co-workers indicate that a similar FCC/HCP crystal will show larger intensity in the top and bottom spots at low shear rates (6.6 s^{-1}) and lower intensity for the same spots at higher shear rates (>66 s^{-1}).[21] Therefore, it is possible that the silica particles could lower the shear rate at which this transition in anisotropy occurs. Nevertheless, it must be noted that that completely different mechanisms could possibly result in similar features on the diffraction patterns. Therefore, the development of alternative flow models and more experiments are necessary to unambiguously determine the flow mechanism of these composites. Since we are focusing primarily on the shear orientation of these structures and the experimental factors that affect this orientation, we leave the determination of the precise flow mechanism of binary crystals for future work.

When the shear rate of the nanocomposite is increased to 100 s^{-1}, the scattering shows significant loss of alignment (Figure 7c,f). At these conditions the hexagonal pattern in the scattering corresponding to the silica particles disappears completely (Figure 7c), indicating the loss of orientation and long-range order in the silica phase. The scattering profile corresponding to the micelle crystal also shows a decrease in the intensity of the diffraction spots and an increase of the intensity of the isotropic powder ring at high shear rates (Figure 7f). This is indicative of a loss of order and an increase in the

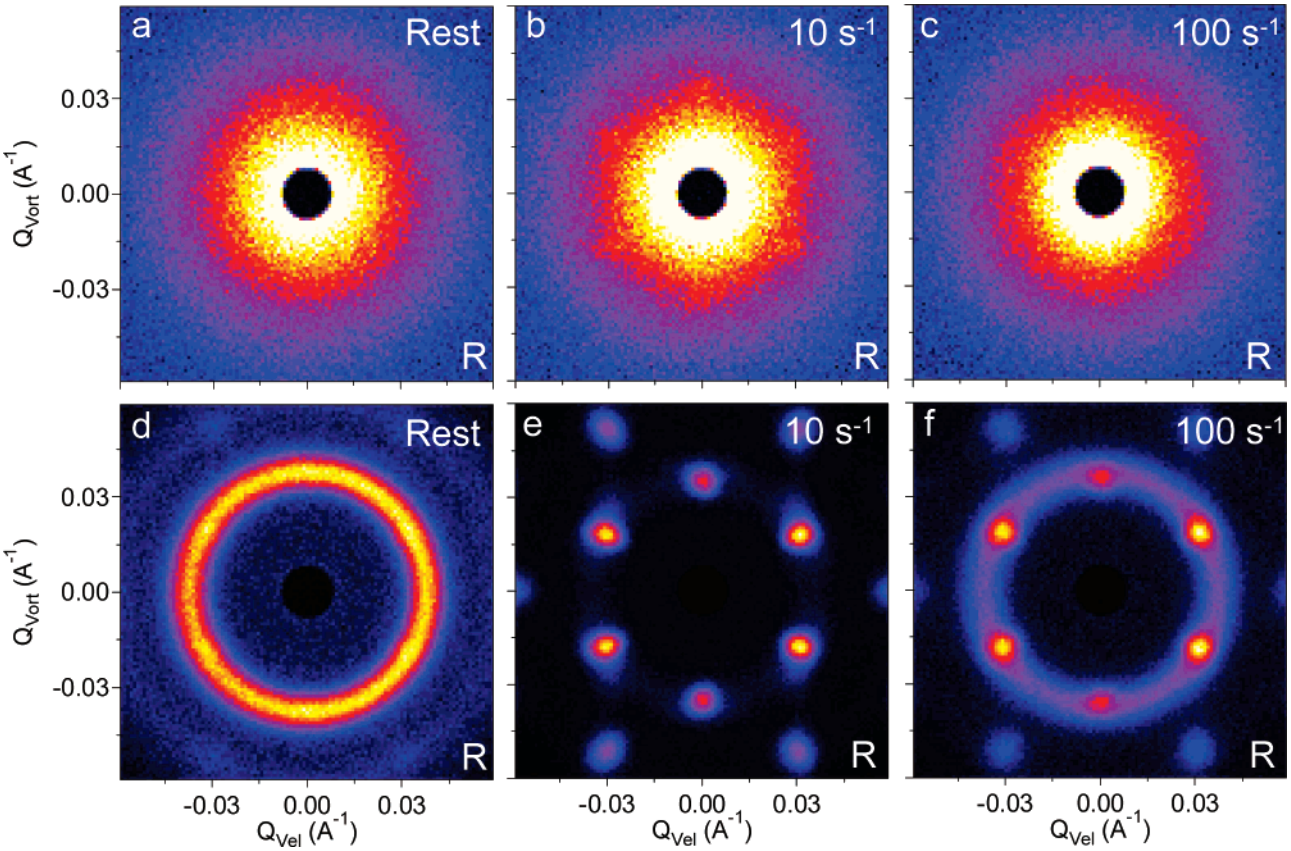

Figure 7. SANS scattering patterns for a nanocomposite sample containing 25 wt % F127 in the matrix and 3 wt % 7 nm silica particles (Ludox SM) at 25 °C. The top profiles correspond to the scattering from the silica particles (polymer matched 12% D_2O) and the bottom profiles to the polymer matrix (silica matched 61% D_2O). The profiles are collected for the samples before shear (a, d) at 10 s^{-1} (b, e) and at 100 s^{-1} (c, f).

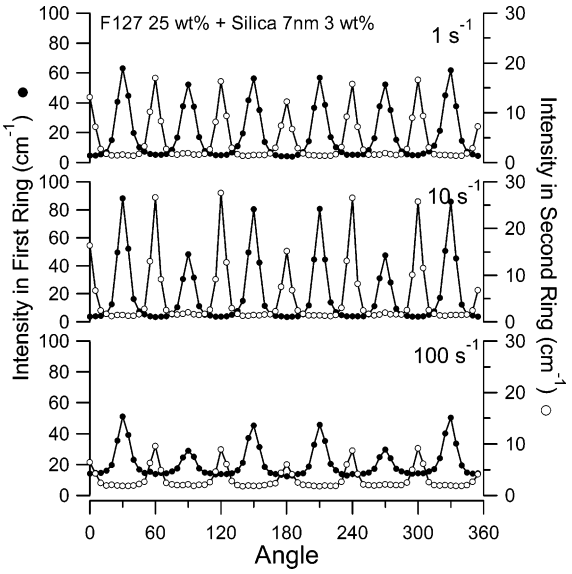

Figure 8. Azimuthal angle average of the intensity of the sample in Figure 7 along the first (closed circles) and second (open circles) hexagonal rings. The scattering corresponds to the micellar phase of the nanocomposite. The angle is measured with respect to the velocity vector.

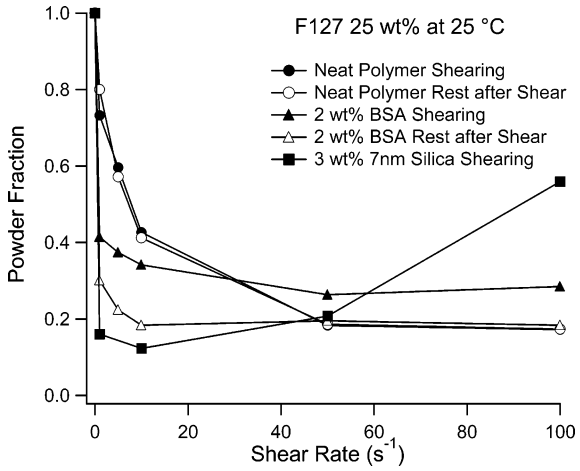

Figure 9. Fraction of the micelles that are not oriented with the shear field (powder fraction) as a function of the applied shear rate for various samples. Closed symbols correspond to the samples under shear, and the open symbols are for the samples at rest immediately after shearing at a specified rate.

powder volume fraction (ϕ_P) in the sample. In contrast, the single-component micellar crystal does not show an increase in the isotropic powder ring at shear rates that are up to 3 times higher (300 s^{-1}). Therefore, in order to obtain the best alignment of these silica composites, it is essential that an intermediate shear rate be used to align the samples.

Equation 3 is used to estimate the fraction of sample that is not oriented with the shear field (powder fraction). The data shown in Figure 9 quantify the extent of shear orientation of the micellar phase of all samples at various shear conditions. Two interesting features become evident from Figure 9. The first observation is that the addition of the silica particles (filled squares) to the micelle crystal leads to significant orientation at significantly lower shear rates than for the neat polymer micelle crystal (filled circles). This is most likely a consequence of the intercalation of the silica particles between the hexagonally close-packed micelle layers. The flow mechanisms for nanocomposites with intercalated particles are expected to have higher energies than those that occur in single-component

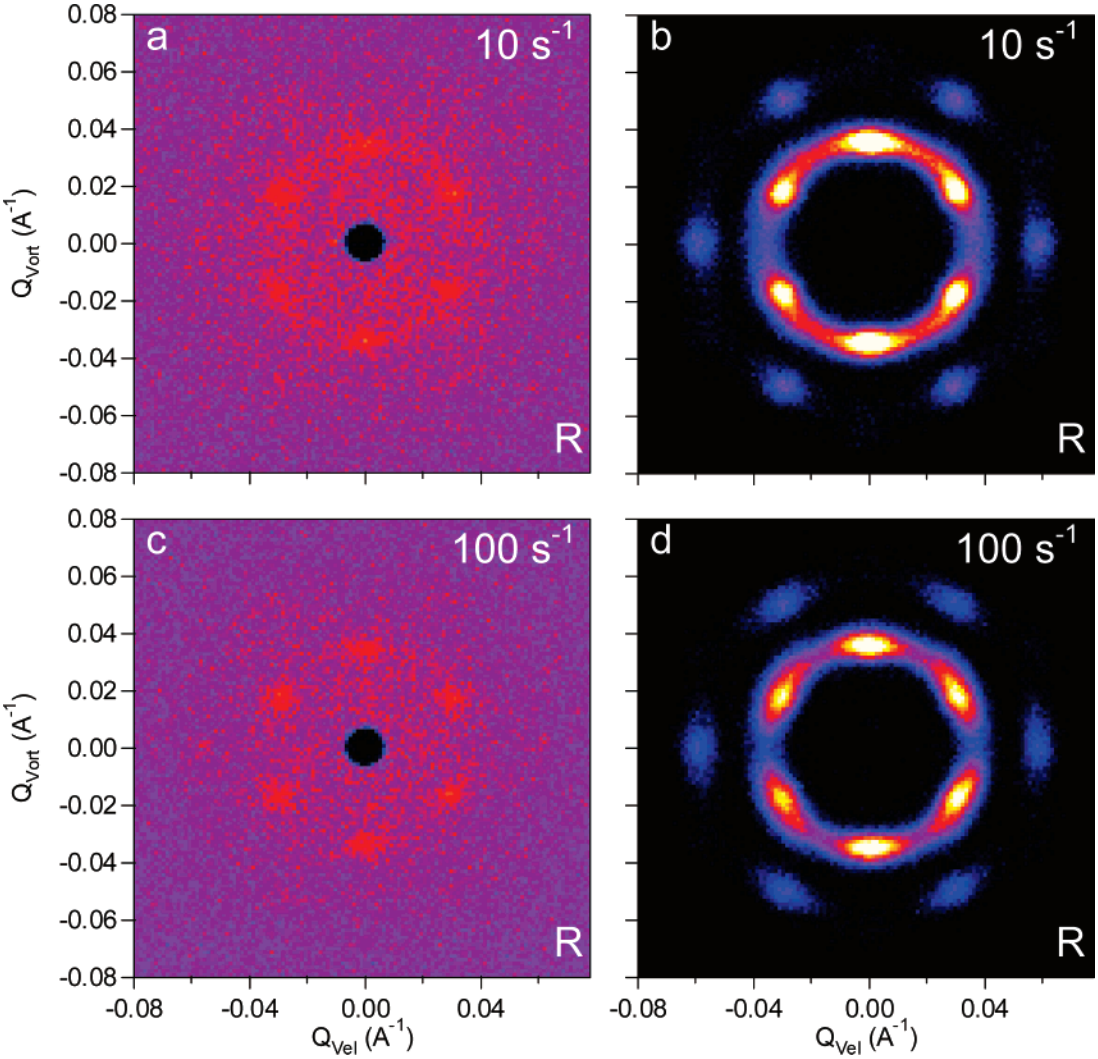

Figure 10. SANS patterns for the scattering of a nanocomposite containing 25 wt % F127 in the matrix and 2 wt % of dispersed BSA at 25 °C. The scattering patterns are collected for the templated protein phase (polymer matched 12% D_2O) and for the micelle crystal phase (protein matched 40% D_2O).

crystals (Figure 1). Therefore, for a specific applied strain, the stress buildup is expected to be larger in nanocomposite samples than in pure micelle crystals which can more efficiently release the stress by sliding layers. For this reason, it is expected that a lower strain (or strain rate) will be sufficient to provide a suitable aligning force. This also explains the increase in modulus and the lower compliance values that are observed for nanocomposites at moderate particle loadings in comparison to the pure micelle crystals.[11]

The second observation that is made from Figure 9 is that, at increasingly higher shear rates, the powder fraction of the silica nanocomposite starts to increase while the powder fraction for the neat micelle crystal reaches a constant value close to 20% powder. This loss of organization is analogous to the shear melting effect that is observed in colloidal crystals at very high shear rates.[8,17,22] Any of these flow mechanisms will have a characteristic time scale associated with it. An order−disorder transition is expected when the imposed strain is increased at a rate that cannot be supported by the flow mechanism. At high rates, the micelles are unable to accommodate themselves in an equilibrium state (low energy) before they are displaced again by the external field, and this leads to a disordering effect.

Figure 10 shows the scattering patterns corresponding to a nanocomposite with BSA proteins as the templated particles. The scattering corresponding to both the micelle crystal and the templated protein phase of the same nanocomposite sample are shown at contrast matching conditions. Unlike the silica, the proteins are monodisperse and lead to improved overall alignment and crystal formation. The polymer used in this work (Pluronic F127) does not interact with the proteins, and thus we should only expect that there will be steric interactions.[34] In Figure 10 it is evident that the hexagonal pattern corresponding to the templated proteins is much sharper than that of the silica particles. This is due in part to the monodispersity of the proteins. Similar alignment is obtained when lysozyme is dispersed in micelle crystals (data not shown). Our ability to see similar behavior with both silica nanoparticles and globular proteins demonstrates the simplicity and versatility of this method in organizing nanosized particle additives into crystalline lattices with long-range order and a dominant orientation.

The observation of a sharp hexagonal pattern corresponding to the first hexagonal ring indicates that the structure of the templated particles is not pure FCC but rather FCC/HCP or pure HCP. The scattering corresponding to the micelle crystal phase also shows the expected hexagonal patterns with the first two hexagonal rings being clearly resolved. Interestingly, the shear-aligned patterns corresponding to the micelle crystal phase of this sample have a similar type of Bragg peak anisotropy as that of the neat micelle crystal (Figure 5) and opposite to the nanocomposite that contains silica (Figure 7). This result

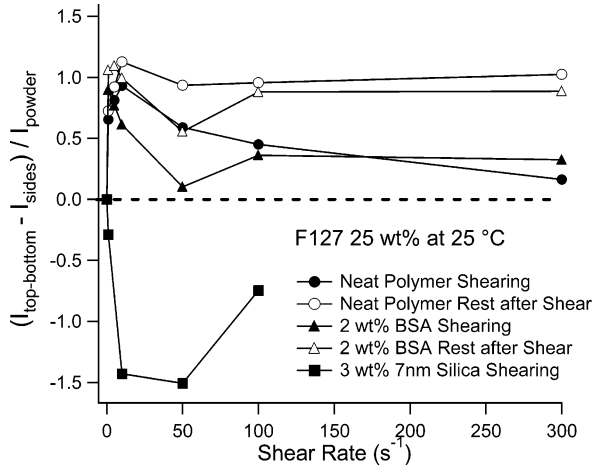

Figure 11. Anisotropy (*A*) of the Bragg spots in the first diffraction ring for various samples as a function of shear rate. The anisotropy is quantified as the difference in intensity of the two top and bottom peaks and the four side peaks with respect to the peak intensity of the powder. Closed symbols represent the samples under shear, and open symbols are for the samples at rest after shearing at a specific rate.

suggests that there is a significant difference between the shear alignment of samples containing dispersed silica and samples containing proteins. This could be due to small differences in particle size. Another possibility is that this difference is due to the interaction of the polymer with the surface of the particles. PEO−PPO copolymers are known to adsorb to silica. Although the adsorption is relatively weak (<0.4 mg/m^2), it still shows that there is some affinity between the surface of the particles and the PEO blocks.[35,36] In contrast, the interaction between PEO−PPO copolymers and the proteins (BSA and lysozyme) is purely repulsive.[34] Therefore, it is possible that the differences in the scattering are due to the attraction of the micelles and the templated particles. The use of particles that have identical size and shape but with different surface chemistry (for example, gold colloids with different thiol ligands) would be an ideal test for the influence of surface interactions.

As discussed previously, the scattering from pure micelle crystals and binary crystal nanocomposites shows shear-dependent differences in the intensity of the Bragg spots of the first-order ring (anisotropy). These differences in peak intensity are related to the flow mechanism and the equilibrium structure of these materials. Therefore, we quantify the anisotropy for all the samples using eq 1 and plot the results in Figure 11 to extract some of this information. In Figure 11 we see that the anisotropy factor for the neat polymer crystal increases rapidly above zero at low shear rates and then decreases again at higher rates. At 300 s^{-1} the anisotropy of the neat crystal almost disappears. Unfortunately, sample tearing prevented the use of larger shear rates. The binary crystal sample with silica particles shows a negative anisotropy factor that reaches a minimum at 50 s^{-1}. The sample that contains dispersed proteins (BSA) shows changes in the anisotropy factor (*A*) with shear and also when shear stops (Figure 11). The shear dependence of the anisotropy factor is similar to that of the neat micelle crystal and has an opposite sign to the anisotropy of the silica nanocomposite. As with the neat micelle crystal, the value of *A* increases when the sample is at rest after shear.

The change in alignment of the binary crystal that contains protein is also calculated and shown in Figure 9. Like the silica nanocomposite, this sample also shows a sharp decrease in the powder fraction at low shear rates when it is compared to the neat micelle crystal. Therefore, alignment occurs at a lower shear rate than in the neat micelle crystal. Still, the minimum powder fraction for the sample under shear is significantly larger ($\phi_P \sim 0.3$) than of the silica composite ($\phi_P \sim 0.12$) and the neat micelle crystal ($\phi_P \sim 0.2$). Interestingly, the powder fraction decreases significantly at rest when shear stops ($\phi_P \sim 0.2$). This indicates that there is a better state of alignment at rest. In contrast, the pure micelle crystal does not show a significant change in the value of ϕ_P during shear and at rest after shear. Also in contrast to the silica composite, the crystal containing proteins does not show a significant loss of alignment at the highest shear rates that are used (up to 300 s^{-1}).

The nature of the shear field applied is important in controlling orientation as seen when sinusoidal oscillations of the strain are used to align the samples rather than steady shear. Figure 12 shows the radial scattering profiles for a protein nanocomposite that is sheared using steady shear and also oscillatory motion. The scattering corresponds to the templated protein phase (polymer matched). We observe that it is difficult to align the crystals from the powder state while subjecting the samples simply to oscillations. Nevertheless, we find that after partial alignment using steady shear, the level of organization that is achieved with oscillatory motion is much higher than that that is achieved using steady shear alone. Additionally, we find that the frequency and amplitude of the oscillations have a remarkable impact on the resulting structures. For example, by using small strain amplitudes (10% strain), it is possible to align the crystals so that that the majority of the hexagonal planes are stacked into an FCC lattice (Figure 12b,c). This is observed in the profiles by the suppression of the first-order hexagonal ring. These profiles are comparable to the predictions of the scattering model for purely FCC lattices (Figure 3a).[23] Similar observations have also been made in similar single-component micellar crystals.[7]

These results suggest that oscillatory shear is more powerful for aligning nanocomposites of this kind. They also demonstrate that it can also be used to tune the organization of the crystals through a judicious choice of shear conditions. The observation of an intense second-order hexagon also indicates that the second-order Bragg spots are not limited by the incoherent background or the instrument resolution. Therefore, the lack of a second-order hexagonal ring in similar samples (Figure 10) is due a lower degree of crystal order and orientation.

In order to use these materials in any real applications, it is also essential that the shear-induced organization persists over a significant period of time at rest. This persistence of order is probed using a sample containing 3 wt % of 7 nm silica particles in a matrix of 30 wt % F127. The solvent contrast is chosen to match the polymer micelles (12% D_2O), and therefore the scattering corresponds to the lattice structure of the templated silica particles. The scattering is collected using a small plate−plate shear cell. This small cell is designed to fit into the standard multicell sample holder of the SANS instrument. This allows us to keep the aligned samples in this portable shear cell over very long periods of time. The sample is shear aligned by manually sliding one of the two quartz plates in the vertical direction. The small shear cell is then sealed and placed in a humidified jar to prevent sample evaporation. The sample is sheared 1 month before the experiment. A large polymer concentration (30 wt %) is used to prevent "melting" of the structure due to fluctuations in the room temperature during this long equilibration period. The resulting profile of the sample after 1 month of storage at rest is shown in Figure 13. Figure 13 clearly shows that the shear alignment is stable for periods as large as 1 month. In fact, the sharp spots in the first hexagonal

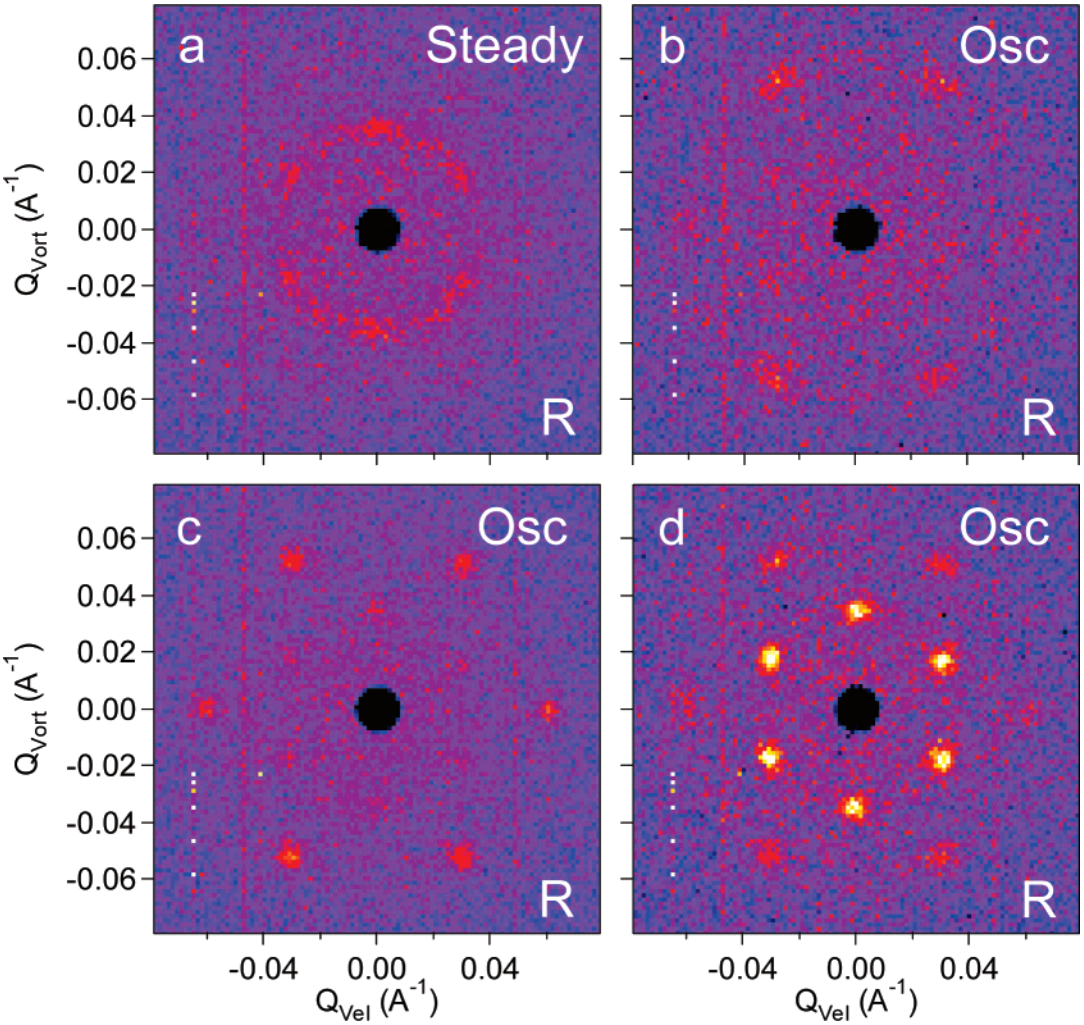

Figure 12. SANS profiles in the radial direction for a nanocomposite sample containing 25 wt % F127 and 3 wt % BSA in a solvent of 12% D_2O (polymer matched): (a) sample under steady shear at a rate of 3 s^{-1}, (b) oscillatory shear with frequency 10 Hz and 10% strain amplitude, (c) oscillatory shear with frequency 0.1 Hz and 10% strain amplitude, and (d) oscillatory shear with frequency of 10 Hz and 100% strain amplitude.

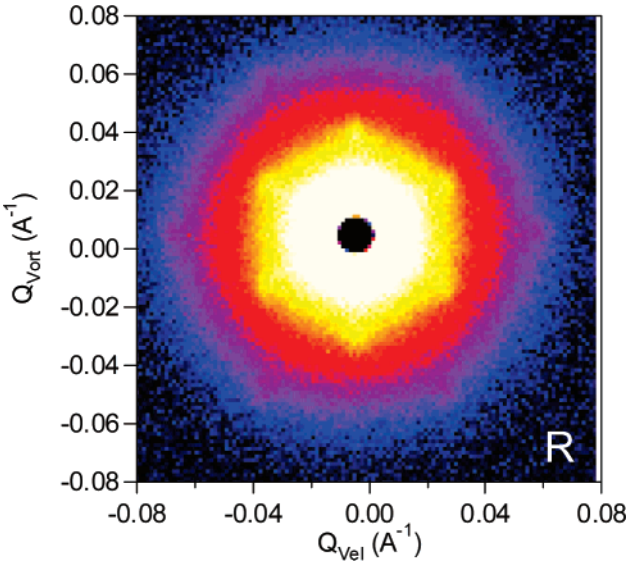

Figure 13. Scattering profile for a sample containing 30 wt % F127 and 3 wt % dispersed silica particles. The sample is in scattering contrast with the silica (polymer is matched). The scattering data are collected from a sample that is shear-aligned manually in a parallel plate shear cell and is then stored for 1 month at room temperature.

ring and the observation of spots in the second ring suggest that the degree of order is even larger than that of corresponding samples under shear (Figure 7b). This improved alignment is not due to the larger polymer concentration because an identical sample is also tested in the concentric cylinder shear cell and the profiles are similar to those shown in Figure 7. The experiment demonstrates that the shear alignment of the templated particles persist at rest for time frames as long as 1 month.

Finally, it is important to note that the samples that are characterized in this work are chosen to have a composition that optimizes the templating order of the nanosized particles. In our previous papers we evaluated the influence of particle stoichiometry, among other controllable parameters, and show that it has a profound effect on the structure and rheology of the binary crystals.[11,12] We find a disordering effect when the number of particles that are dispersed in the matrix greatly exceeds the stoichiometry of one particle per template site. When we probe the structure of overloaded samples under shear, we find that there is no alignment and the scattering does not show any signs of crystalline orientation or long-range order. Therefore, it is important to carefully control the composition of the samples in order to obtain well-organized binary crystals. We have extensively characterized the influence of these important parameters and their influence on the structure and macroscopic properties of these novel materials.[11,12]

5. Conclusions

We present a thorough investigation of the factors that affect the alignment of binary crystals of micelles and nanosized particles. The macroscopic alignment of both phases that make up these cocrystals is demonstrated for the first time using shear fields and contrast variation SANS experiments. This macroscopic shear orientation is expected to provide a valuable tool in the design of novel nanostructured materials with controllable properties. We also probe the influence of shear rate on the overall level of organization in the samples. It is found that binary crystals align at shear rates that are much lower than those required for neat micelle crystals. However, it is also found that high shear rates can result in the loss of long-range order of binary crystals while the neat micelle crystals remain aligned. Shear orientation is also demonstrated using different types of dispersed particles, indicating that the method is robust and versatile.

The diffraction patterns of the oriented crystals are also compared to a model for colloidal crystals under shear. This comparison reveals important differences that are possibly caused by an unaccounted crystal phase that coexists in the oriented samples. Finally, we present a new simple method to quantify the level of alignment of oriented crystals using the diffraction patterns. This allows the quantification of the alignment without the need to use a complex model to fit the two-dimensional diffraction patterns.

Acknowledgment. We acknowledge the PPG foundation and National Science Foundation (CTS-9871110) for equipment. D.C.P. acknowledges the PPG and the Lubrizol foundations for providing research funding. We are very grateful to Dr. Lionel Porcar (NIST) for his help during the SANS experiments and for his input in this work. This work utilized facilities supported in part by the National Science Foundation under Agreement DMR-9986442. We acknowledge the support of the National Institute of Standards and Technology, U.S. Department of Commerce, in providing the neutron research facilities used in this work.

Supporting Information Available: Detector profile for a sample containing 25 wt% Pluronic F127 (Figure A) and circularly averaged SANS profiles for samples containing 25 wt% Pluronic F127 (Figure B). This material is available free of charge via the Internet at http://pubs.acs.org.

References and Notes

(1) Alexandridis, P.; Hatton, T. A. *Colloids Surf., A* **1995**, *96*, 1−46.
(2) Wanka, G.; Hoffmann, H.; Ulbricht, W. *Macromolecules* **1994**, *27*, 4145−4159.
(3) Bates, F. S.; Fredrickson, G. H. *Phys. Today* **1999**, *52*, 32−38.
(4) Forster, S.; Antonietti, M. *Adv. Mater.* **1998**, *10*, 195.
(5) Versmold, H.; Musa, S.; Dux, C.; Lindner, P.; Urban, V. *Langmuir* **2001**, *17*, 6812−6815.
(6) Shevchenko, E. V.; Talapin, D. V.; Murray, C. B.; O'Brien, S. *J. Am. Chem. Soc.* **2006**, *128*, 3620−37.
(7) Molino, F. R.; Berret, J. F.; Porte, G.; Diat, O.; Lindner, P. *Eur. Phys. J. B* **1998**, *3*, 59.
(8) Park, M. J.; Bang, J.; Harada, T.; Char, K.; Lodge, T. P. *Macromolecules* **2004**, *37*, 9064−9075.
(9) Mortensen, K. *J. Phys.: Condens. Matter* **1996**, *8*, A103−A124.
(10) Bockstaller, M. R.; Mickiewicz, R. A.; Thomas, E. L. *Adv. Mater.* **2005**, *17*, 1331−1349.
(11) Pozzo, D. C.; Hollabaugh, K. R.; Walker, L. M. *J. Rheol.* **2005**, *49*, 759−782.
(12) Pozzo, D. C.; Walker, L. M. *Macromol. Symp.* **2005**, *227*, 203−210.
(13) Pozzo, D. C.; Walker, L. M. *Colloids Surf., A* **2006**, *294*, 117−129.
(14) Maier, S. A.; Brongersma, M. L.; Kik, P. G.; Meltzer, S.; Requicha, A. A. G.; Atwater, H. A. *Adv. Mater.* **2001**, *13*, 1501.
(15) Matsui, J.; Akamatsu, K.; Nishiguchi, S.; Miyoshi, D.; Nawafune, H.; Tamaki, K.; Sugimoto, N. *Anal. Chem.* **2004**, *76*, 1310−1315.
(16) Abbas, S.; Lodge, T. P. *Phys. Rev. Lett.* **2006**, *97*, 097803.
(17) Hamley, I. W.; Daniel, C.; Mingvanish, W.; Mai, S. M.; Booth, C.; Messe, L.; Ryan, A. J. *Langmuir* **2000**, *16*, 2508−2514.
(18) Bang, J.; Lodge, T. P.; Wang, X. H.; Brinker, K. L.; Burghardt, W. R. *Phys. Rev. Lett.* **2002**, *89*.
(19) Eiser, E.; Molino, F.; Forte, G.; Pithon, X. *Rheol. Acta* **2000**, *39*, 201−208.
(20) Ackerson, B. J.; Pusey, P. N. *Phys. Rev. Lett.* **1988**, *61*, 1033−1036.
(21) Mcconnell, G. A.; Lin, M. Y.; Gast, A. P. *Macromolecules* **1995**, *28*, 6754−6764.
(22) Dux, C.; Musa, S.; Reus, V.; Versmold, H.; Lindner, P. *J. Chem. Phys.* **1998**, *109*, 2556.
(23) Loose, W.; Ackerson, B. J. *J. Chem. Phys.* **1994**, *101*, 7211−7220.
(24) Straty, G. C.; Hanley, H. J. M.; Glinka, C. J. *J. Stat. Phys.* **1991**, *62*, 1015−1023.
(25) Straty, G. C.; Muzny, C. D.; Butler, B. D.; Lin, M. Y.; Slawecki, T. M.; Glinka, C. J.; Hanley, H. J. M. *Physica B* **1997**, *241*, 74−76.
(26) Glinka, C. J.; Barker, J. G.; Hammouda, B.; Krueger, S.; Moyer, J. J.; Orts, W. J. *J. Appl. Crystallogr.* **1998**, *31*, 430−445.
(27) Kline, S. R. *J. Appl. Crystallogr.* **2006**, *39*, 895−900.
(28) Solomon, T.; Solomon, M. J. *J. Chem. Phys.* **2006**, *124*, 13905.
(29) E. Trizac, M. D. Eldridge, P. A. Madden, *Mol. Phys.* **1997**, *90*, 675−678.
(30) Hunt, N.; Jardine, R.; Bartlett, P. *Phys. Rev. E* **2000**, *62*, 900−913.
(31) Figure is included in the Supporting Information.
(32) Dolbnya, I. P.; Petukhov, A. V.; Aarts, D. G. A. L.; Vroege, G. J.; Lekkerkerker, H. N. W. *Europhys. Lett.* **2005**, *72*, 962−968.
(33) Eiser, E.; Molino, F.; Porte, G.; Diat, O. *Phys. Rev. E* **2000**, *61*, 6759−6764.
(34) Almeida, N. L.; Oliveira, C. L. P.; Torriani, I. L.; Loh, W. *Colloids Surf., B* **2004**, *38*, 67−76.
(35) Malmsten, M.; Linse, P.; Cosgrove, T. *Macromolecules* **1992**, *25*, 2474−2481.
(36) Shar, J. A.; Obey, T. M.; Cosgrove, T. *Colloids Surf., A* **1999**, *150*, 15−23.

MA0700173